Original Article

Institution of MECHANICAL ENGINEERS
Journal of MECHANICAL ENGINEERING SCIENCE

Proc IMechE Part C:
J Mechanical Engineering Science
0(0) 1–11

DOI: 10.1177/0954406218786978
journals.sagepub.com/home/pic
SAGE

Design and kinematic analysis of a spherical parallel manipulator using concurrent planar parallelogram linkages

Genliang Chen[1,2], Weidong Yu[1,2], Hao Wang[1,2] and Jiepeng Wang[1,2]

Abstract

This paper presents the design of a novel spherical parallel manipulator. The spherical parallel manipulator consists of three identical limbs and each of them is formed by a planar parallelogram linkage, a universal joint, and a revolute one, successively. Its mobility is analyzed using the reciprocal screws. After that, the kinematics is analyzed in detail, including inverse kinematic modeling, which is validated by a numerical example, inverse Jacobian analysis, singularity analysis, and manipulability analysis, which shows a relatively good performance of force transmission. Then based on the analysis, one prototype is fabricated to validate the effectiveness and feasibility of the design. In the end, some conclusions are drawn and future works are discussed.

Keywords

Spherical parallel manipulator, parallelogram linkage, reciprocal screws, kinematics, prototype

Date received: 26 October 2017; accepted: 8 June 2018

Introduction

A spherical parallel manipulator (SPM) is a manipulator that has three degrees of freedom (DOFs) and can rotate about a fixed point in any direction. The SPMs can be classified into the overconstrained and nonoverconstrained ones. The most famous overconstrained architecture is the 3-RRR (for simplicity, in this paper R stands for revolute joint, P for prismatic joint, U for universal joint, C for cylindrical joint, and S for spherical joint) architecture, which is proposed by Gosselin and Angeles,[1] so called the agile eye.[2] In the architecture, all the axes of the revolute joints intersect with a fixed point.

Compared to the literature on overconstrained SPMs, the literature on nonoverconstrained ones are more plentiful. Some representative ones are as follows. Vischer et al.[3] proposed a novel SPM in which each limb consists of a S joint, a Pa (planar parallelogram) joint, and an R joint from the end effector to the base. Di Gregorio et al.[4–6] proposed several SPMs, including the 3-URC, the 3-RUU, and the 3-RRS SPMs. Moreover, they also disclosed that the 3-RRPRR architectures can perform spherical motion when they match specified geometric conditions.[7] Karouia et al.[8] disclosed that the 3-UPU architecture can perform 3-DOF spherical motion when two revolute pairs of the two U joints converge at a fixed point. By utilizing Lie group, they[9] also found a family of nonoverconstrained SPMs whose limbs are made of five serial-connected lower kinematic pairs. Li et al.[10] disclosed a family of SPMs in which each limb consists of five R joints and three of them pass through a fixed point. By combining the traditional 3-RRR overconstrained SPM and the Delassus linkages, Kong et al.[11] identified several new nonoverconstrained SPMs. Fang et al.[12] enumerated the feasible limb structures based on the reciprocal screws and synthesized a class of SPMs. Karouia et al.[13] synthesized a number of asymmetrical SPMs in which the limbs are structurally distinct. They also disclosed some nonoverconstrained SPMs such as the 3-RCC, 3-CCR, and 3-CRC architectures.[14] Gallardo et al.[15] investigated a family of nonoverconstrained SPMs consisting of one passive spherical joint and two limbs. Mohammadi et al.[16] disclosed a double-triangle

[1]State Key Laboratory of Mechanical System and Vibration, Shanghai Jiao Tong University, Shanghai, PR China
[2]Shanghai Key Laboratory of Digital Manufacture for Thin-walled Structures, Shanghai Jiao Tong University, Shanghai, PR China

Corresponding author:
Hao Wang, State Key Laboratory of Mechanical System and Vibration, Shanghai Jiao Tong University, Room 611, Mechanical Building A, No. 800, Dongchuan Rd., Shanghai 200240, PR China.
Email: wanghao@sjtu.edu.cn

SPM, based on which, Enferadi et al.[17] proposed the single-triangle SPM. Huda et al.[18] designed a 3-URU SPM and optimized its dimensional parameters to obtain a large workspace. Callegari et al.[19] investigated the 3-CPU SPM and analyzed its kinematics and dynamics in detail. Lin et al.[20] proposed the concept of the upper-lower combination and synthesized some novel symmetrical SPMs. Enferadi et al.[21] proposed the 3(RSS)-S SPM whose revolute joints are set coaxial. Some SPMs in which the moving platform is connected to the base by three identical limbs and one fixed S joint can also be found.[22–24]

Although there exist extensive researches about SPMs for various applications, they are nowhere near enough and novel SPMs for practical applications are still worth investigating. In this paper, a new type of 3-DOF SPM is proposed by taking advantage of the planar parallelogram linkage. The proposed parallel manipulator constitutes three identical limbs, each of which consists of a planar parallelogram linkage, a universal joint and a revolute one, successively. Therefore, it is termed as 3-PaUR parallel manipulator in this paper. Its kinematics is analyzed in detail and a prototype is fabricated to demonstrate the feasibility of the design. Most of the previously introduced currently available SPMs consist of prismatic joints or spherical joints. However, the proposed SPM in this paper can be established only by revolute joints, which can significantly reduce the manufacturing costs.

This paper is organized as follows. The upcoming section presents the architecture of the proposed SPM and its mobility analysis. Then, the kinematics analysis is presented where both the inverse kinematics and inverse Jacobian matrix are discussed. Next, the singularity analysis of the proposed SPM is presented and the manipulability analysis is carried out. Following section is devoted to the presentation of the fabricated prototype, the limitations of the proposed SPM, and discussion of future works. Finally, some conclusions are drawn in the last section.

Architecture description and mobility analysis

In this section, the architecture of the proposed parallel manipulator is presented. In addition, mobility of the studied spatial parallel manipulator is analyzed based on the theory of reciprocal screws.

Architecture description

In the manipulator, the lying planes of the parallelogram linkages are denoted by $\mathscr{P}_i$, $i = 1, 2, 3$, as shown in Figure 1. The first axis of the corresponding universal joint, denoted by the unit vector $\boldsymbol{u}_i \in \mathbb{R}^3$, is perpendicular to $\mathscr{P}_i$. While $\boldsymbol{v}_i \in \mathbb{R}^3$ is used to represent the direction of the U-joint's second axis. Since $\boldsymbol{v}_i$ is perpendicular to $\boldsymbol{u}_i$, the second axis of universal joint

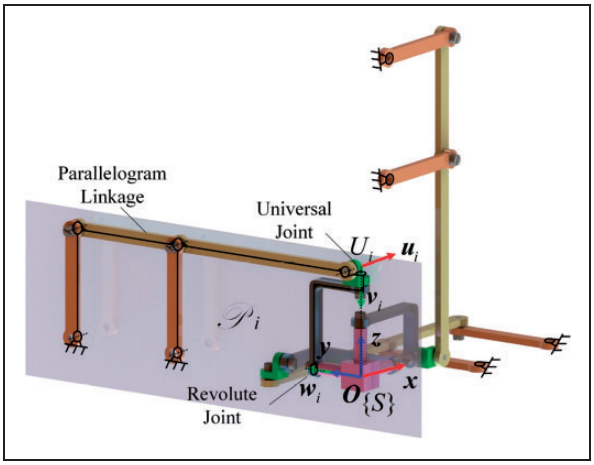

Figure 1. Schematic diagram of the proposed parallel manipulator.

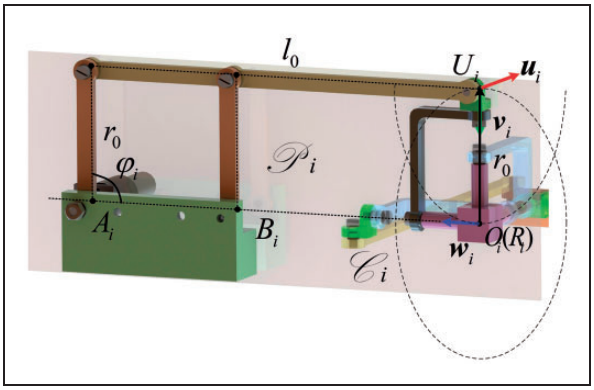

Figure 2. Kinematic structure of the -PaUR limb.

is constrained within $\mathscr{P}_i$. Meanwhile, the direction of the revolute joint is denoted by the unit vector $\boldsymbol{w}_i \in \mathbb{R}^3$, which is always orthogonal to $\boldsymbol{v}_i$.

According to the Pa-linkage's constraint, the position of the universal joint, denoted by U_i, is constrained on a circle on the plane $\mathscr{P}_i$, represented by $\mathscr{C}_i$ as illustrated in Figure 2. The center of $\mathscr{C}_i$, denoted by O_i, lies on the line $\overline{A_iB_i}$, where A_i and B_i are the positions of the Pa-linkage's revolute joints connected to the frame. Obviously, the distance between O_i and A_i is simply the length of coupler link in the Pa-linkage, namely l_0 as shown in the figure. And the radius of $\mathscr{C}_i$ just equals to the length of crank link, namely r_0. Moreover, the length of the link between the universal and revolute joints, namely $\overline{U_iR_i}$, is also set to r_0. Here, R_i denotes the intersecting point between the axes $\boldsymbol{v}_i$ and $\boldsymbol{w}_i$, as shown in the figure. Thus, $\overline{U_iR_i}$ can be regarded as the common perpendicular of the axes associated with $\boldsymbol{u}_i$ and $\boldsymbol{w}_i$. Moreover, all those points R_i, $i = 1, 2, 3$ are supposed to be coincident with each other. In other words, all the revolute joints on the moving platform intersect at a common point, which is denoted as O_0.

In the proposed parallel manipulator, the rotations of the Pa-linkages' cranks are assigned as the

actuations. Then, in each limb, the position of universal joint relates to a specific point on $\mathscr{C}_i$ for any given input of the corresponding crank. Since $\boldsymbol{v}_i$ is constrained within $\mathscr{P}_i$, the point R_i (namely O_0) will be confined on a circle on $\mathscr{P}_i$, which is centered at U_i and passes through O_i, as shown in Figure 2.

In order to assemble the limbs together, the center points O_1, O_2, and O_3 are set to be coincident with each other, which is denoted by O. As a result, for any given set of the inputs, all the circular trajectories for R_i, $i=1, 2, 3$ commonly pass through O. Thus, the fixed point O permanently becomes a common intersection of the above circles for any given configuration. Therefore, the center point O_0 on the manipulator's moving platform will be constrained at O permanently. In other words, the moving platform of the proposed parallel manipulator does not possess translational mobilities.

It should be noted that the lines $\overline{A_iB_i}$, $i = 1, 2, 3$ can be intersected at arbitrary angles, as long as they pass through the common point O. For the simplification of discussion, the orthogonal situation is adopted in this paper to make the analysis easy to understand. Thus, the limb planes $\mathscr{P}_1$, $\mathscr{P}_2$, and $\mathscr{P}_3$ are mutually perpendicular to each other and intersected at the common point O. And $\mathscr{C}_i, i = 1, 2, 3$ correspond to three orthogonal great circles of the sphere $\mathscr{S}_i$, which is centered at O and has the radius of r_0. Meanwhile, the axes of the revolute joints, namely $\boldsymbol{w}_i$, $i = 1, 2, 3$ are also mutual-orthogonally intersected at O_0.

As illustrated in the figure, let {S} be the system inertia frame, which is located at O and having its coordinate axes $\boldsymbol{x}$, $\boldsymbol{y}$, and $\boldsymbol{z}$ parallel to $\boldsymbol{u}_1$, $\boldsymbol{u}_2$ and $\boldsymbol{u}_3$, respectively. Thus, the limbs are lying on the $\boldsymbol{yz}$ ($\mathscr{P}_1$), $\boldsymbol{zx}$ ($\mathscr{P}_2$), and $\boldsymbol{xy}$ ($\mathscr{P}_3$) planes of {S}, respectively. Meanwhile, let {T} be the manipulator's tool frame attached to the moving platform at O_0 and have its axes coincident with $\boldsymbol{w}_3$, $\boldsymbol{w}_1$, and $\boldsymbol{w}_2$, respectively. Therefore, the tool frame {T} will be coincident with the inertia one {S} at the initial configuration. And the moving platform ({T}) can only rotate with respect to {S} about the fixed point O, which will be discussed in the following section.

Mobility analysis

In this section, the theory of reciprocal screws[25,26] is used to analyze the mobility of the 3-PaUR parallel manipulator presented in the above.

From kinematics point of view, the planar parallelogram linkage in the limbs can be equivalently modeled as a virtual revolute joint located at O and parallel to $\boldsymbol{u}_i$. Then, the PaUR-limb can be considered as a RUR limb and the corresponding twist system can be represented as

$$\mathbb{S}_i = \text{span}\{\boldsymbol{S}_{i,1}, \boldsymbol{S}_{i,2}, \boldsymbol{S}_{i,3}, \boldsymbol{S}_{i,4}\} \tag{1}$$

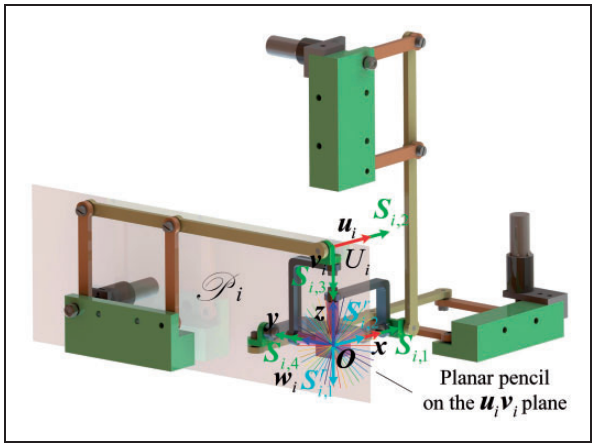

Figure 3. Screw system of the PaUR limbs.

where $\boldsymbol{S}_{i,1} = \begin{bmatrix} \boldsymbol{u}_i \\ \boldsymbol{0} \end{bmatrix}$ denotes the joint twist associated with the parallelogram linkage which is equivalent to a revolute joint parallel to $\boldsymbol{u}_i$ and passing through the origin O of {S}.

$\boldsymbol{S}_{i,2} = \begin{bmatrix} \boldsymbol{u}_i \\ \boldsymbol{r}_{U_i} \times \boldsymbol{u}_i \end{bmatrix}$, $\boldsymbol{S}_{i,3} = \begin{bmatrix} \boldsymbol{v}_i \\ \boldsymbol{0} \end{bmatrix}$ are the joint twists associated with the universal joint's axes. Here, $\boldsymbol{r}_{U_i} = -r_0\,\boldsymbol{v}_i$ denotes the position vector U_i with respect to {S}, as shown in Figure 3.

$\boldsymbol{S}_{i,4} = \begin{bmatrix} \boldsymbol{w}_i \\ \boldsymbol{0} \end{bmatrix}$ represents the joint twist of the revolute joint which is in the direction $\boldsymbol{w}_i$ and passing through O. It should be noted that all the screw elements in this paper are represented with respect to the system's inertia frame {S}.

From equation (1), it is obvious that $\boldsymbol{S}_{i,1}$, $\boldsymbol{S}_{i,3}$, and $\boldsymbol{S}_{i,4}$ correspond to three revolute joints passing through the common point O along different directions. Therefore, they can be regarded as a spherical joint located at O. It should be noted that singular configurations are not taken into account in this section. In other words, the axis of the limb's revolute joint will not be parallel to the first axis of the universal one, namely $\boldsymbol{w}_i \neq \boldsymbol{u}_i$.

As a result, the limb's twist system $\mathbb{S}_i$ corresponds to a fourth-order screw system, consisting of a spherical and a revolute joint. By using the observation method,[27] it is not difficult to derive the corresponding reciprocal screw system, namely the limb's constraint screw system, given by

$$\mathbb{S}_i^r = \text{span}\left\{\boldsymbol{S}_{i,1}^r, \boldsymbol{S}_{i,2}^r\right\} \tag{2}$$

where $\boldsymbol{S}_{i,1}^r = \begin{bmatrix} \boldsymbol{0} \\ \boldsymbol{v}_i \end{bmatrix}$ and $\boldsymbol{S}_{i,2}^r = \begin{bmatrix} \boldsymbol{0} \\ \boldsymbol{u}_i \end{bmatrix}$ represent two linearly independent constraint screws applied on the limb, which can be regarded as a set of basis of $\mathbb{S}_i^r$.

It should be noted that the basis of the limb's constraint screw system is not unique. Any pair of linearly independent combinations of $\boldsymbol{S}_{i,1}^r$ and $\boldsymbol{S}_{i,2}^r$ can construct a basis. However, the elements $\boldsymbol{S}_{i,1}^r$ and $\boldsymbol{S}_{i,2}^r$ have a very simple expression and intuitive interpretation. They simply relate to the pure force constraints passing through O and in the directions of $\boldsymbol{u}_i$ and $\boldsymbol{v}_i$, respectively. Therefore, the constraint system $\mathbb{S}_i^r$ relates to a degenerated second-order screw system,[25] whose elements form a planar pencil on the $\boldsymbol{u}_i\boldsymbol{v}_i$ plane and centered at O, as illustrated in Figure 3.

Consequently, for the moving platform of the proposed parallel manipulator, the whole constraint system caused by all the three limbs can be obtained as

$$\begin{aligned}\mathbb{S}^r &= \mathbb{S}_1^r \cup \mathbb{S}_2^r \cup \mathbb{S}_3^r \\ &= \operatorname{span}\left\{\boldsymbol{S}_{1,1}^r, \boldsymbol{S}_{1,2}^r, \boldsymbol{S}_{2,1}^r, \boldsymbol{S}_{2,2}^r, \boldsymbol{S}_{3,1}^r, \boldsymbol{S}_{3,2}^r\right\}\end{aligned} \tag{3}$$

Between any pair of the limbs' constraint systems, there exists a common element which is along the intersection of the corresponding planes. Then, we have

$$\mathbb{S}_1^r \cap \mathbb{S}_2^r = \begin{bmatrix}\boldsymbol{0}\\ \boldsymbol{z}\end{bmatrix}, \quad \mathbb{S}_2^r \cap \mathbb{S}_3^r = \begin{bmatrix}\boldsymbol{0}\\ \boldsymbol{x}\end{bmatrix}, \quad \mathbb{S}_3^r \cap \mathbb{S}_1^r = \begin{bmatrix}\boldsymbol{0}\\ \boldsymbol{y}\end{bmatrix} \tag{4}$$

where $\boldsymbol{x}$, $\boldsymbol{y}$ and $\boldsymbol{z}$ represent the unit vectors associated with the coordinate axes of {S}, which simply correspond to $\boldsymbol{u}_1$, $\boldsymbol{u}_2$, and $\boldsymbol{u}_3$, respectively.

Equation (4) indicates that the proposed spatial 3-PaUR manipulator is an overconstrained parallel manipulator. Then, a set of linearly independent elements can be extracted from equation (3) as the basis of $\mathbb{S}^r$, given by

$$\mathbb{S}^r = \left\{\boldsymbol{S}_1^r,\ \boldsymbol{S}_2^r,\ \boldsymbol{S}_3^r\right\} \Rightarrow \quad \begin{cases}\boldsymbol{S}_1^r = \begin{bmatrix}\boldsymbol{0}\\ \boldsymbol{x}\end{bmatrix}\\ \boldsymbol{S}_2^r = \begin{bmatrix}\boldsymbol{0}\\ \boldsymbol{y}\end{bmatrix}\\ \boldsymbol{S}_3^r = \begin{bmatrix}\boldsymbol{0}\\ \boldsymbol{z}\end{bmatrix}\end{cases} \tag{5}$$

where $\boldsymbol{S}_1^r$, $\boldsymbol{S}_2^r$, and $\boldsymbol{S}_3^r$ are linearly independent of each other.

From equation (5), it is known that the constraint system of the moving platform relates to a degenerate third-order screw system,[25] which corresponds to a bundle of lines through the common point O and having the identical pitch of 0. Then, the corresponding reciprocal system, namely the twist system of the moving platform, can be readily obtained as

$$\mathbb{S} = \operatorname{span}\{\boldsymbol{S}_1, \boldsymbol{S}_2, \boldsymbol{S}_3\} \tag{6}$$

where $\boldsymbol{S}_1 = \begin{bmatrix}\boldsymbol{x}\\ \boldsymbol{0}\end{bmatrix}$, $\boldsymbol{S}_2 = \begin{bmatrix}\boldsymbol{y}\\ \boldsymbol{0}\end{bmatrix}$, $\boldsymbol{S}_3 = \begin{bmatrix}\boldsymbol{z}\\ \boldsymbol{0}\end{bmatrix}$ are a set of basis of the moving platform's twist system.

From equation (6), it is known that the twist screw system of the manipulator's moving platform also relates to a degenerate 3-system, which is centered at O and has the identical pitch of 0. Therefore, the proposed parallel manipulator possesses three rotational degrees-of-freedom about the fixed point O. Moreover, the above result is independent of the exact orientation where the manipulator's moving platform reaches. In other words, the proposed 3-PaUR parallel manipulator has the capability of continuously three-dimensional rotating within its workspace.

Kinematics analysis

In this section, the inverse kinematics of the proposed 3-DOF rotational parallel manipulator is studied. In addition, the corresponding Jacobian matrix is also modeled for the singularity and performance analysis studied in the following sections.

Inverse kinematics

In this paper, the canonical coordinates of the first kind[28] is employed to depict the orientation of the manipulator's moving platform. It can also be regarded as the elements of the Lie algebra $so(3)$ associated with the special orthogonal group $SO(3)$. Let $\boldsymbol{s} = [s_1, s_2, s_3]^T \in \mathbb{R}^3$ be an arbitrary vector with the modulus of $\theta = \|\boldsymbol{s}\|$. Thus, the relative orientation of the moving platform's tool frame {T} with respect to {S} can be obtained through a rotation of θ about the axis associated with $\boldsymbol{s}$.

Then, using the exponential map from $so(3)$ to $SO(3)$, the relative rotation matrix of {T} with respect to {S} can be obtained as

$$\mathbf{R}_{st} = \exp(\hat{\mathbf{s}}) = \mathbf{I}_3 + \frac{1}{\theta}\sin\theta\hat{\mathbf{s}} + \frac{1}{\theta^2}(1-\cos\theta)\hat{\mathbf{s}}^2 \tag{7}$$

where $\mathbf{I}_3$ is the three-order identity matrix. $\hat{\mathbf{s}} \in so(3)$ represents the 3×3 skew-symmetric matrix associated with $\boldsymbol{s}$, which is given by

$$\hat{\mathbf{s}} = \begin{bmatrix}0 & -s_3 & s_2\\ s_3 & 0 & -s_1\\ -s_2 & s_1 & 0\end{bmatrix}$$

Then, according to the definition of {T}, the directions of the moving platform's revolute joints in {S} can be represented as

$$\begin{cases}\boldsymbol{w}_1 = \mathbf{R}_{st}\boldsymbol{e}_2 = \left[w_{1,x},\ w_{1,y},\ w_{1,z}\right]^T\\ \boldsymbol{w}_2 = \mathbf{R}_{st}\boldsymbol{e}_3 = \left[w_{2,x},\ w_{2,y},\ w_{2,z}\right]^T\\ \boldsymbol{w}_3 = \mathbf{R}_{st}\boldsymbol{e}_1 = \left[w_{3,x},\ w_{3,y},\ w_{3,z}\right]^T\end{cases} \tag{8}$$

where $\boldsymbol{e}_1 = [1,0,0]^T$, $\boldsymbol{e}_2 = [0,1,0]^T$ and $\boldsymbol{e}_3 = [0,0,1]^T$ denote the direction vectors of the revolute joints represented with respect to {T}.

By substituting equation (7) into equation (8), an analytical expression of the unit vectors $\boldsymbol{w}_i$ can be obtained as

$$\begin{cases} w_{1,x} = (1-C_\theta)s'_1 s'_2 - s'_3 S_\theta \\ w_{1,y} = (1-C_\theta)s'_2 s'_2 + C_\theta \\ w_{1,z} = (1-C_\theta)s'_3 s'_2 + s'_1 S_\theta \end{cases} \begin{cases} w_{2,x} = (1-C_\theta)s'_1 s'_3 + s'_2 S_\theta \\ w_{2,y} = (1-C_\theta)s'_2 s'_3 - s'_1 S_\theta \\ w_{2,z} = (1-C_\theta)s'_3 s'_3 + C_\theta \end{cases} \begin{cases} w_{3,x} = (1-C_\theta)s'_1 s'_1 + C_\theta \\ w_{3,y} = (1-C_\theta)s'_2 s'_1 + s'_3 S_\theta \\ w_{3,z} = (1-C_\theta)s'_3 s'_1 - s'_2 S_\theta \end{cases} \tag{9}$$

where $C_\theta = \cos\theta$ and $S_\theta = \sin\theta$. While $s'_i = \frac{1}{\theta}s_i, i = 1,2,3$ are components of the unit vector $\boldsymbol{s}' = \frac{1}{\theta}\boldsymbol{s}$.

As indicated in the ''Architecture description and mobility analysis'' section, the unit vector $\boldsymbol{v}_i$ always lies on the plane $\mathscr{P}_i$ according to the limbs' geometric constraint. Meanwhile, it should also be perpendicular to the vector $\boldsymbol{w}_i$. Then, by projecting $\boldsymbol{w}_i$ onto $\mathscr{P}_i$ and rotating it to an orthogonal position, we have

$$\boldsymbol{v}_i = \exp\left(\frac{\pi}{2}\hat{\mathbf{u}}_i\right)\frac{(\mathbf{I}_3 - \boldsymbol{u}_i\boldsymbol{u}_i^T)\boldsymbol{w}_i}{\|(\mathbf{I}_3 - \boldsymbol{u}_i\boldsymbol{u}_i^T)\boldsymbol{w}_i\|} \tag{10}$$

where $\exp\left(\frac{\pi}{2}\hat{\mathbf{u}}_i\right) \in SO(3)$ corresponds to the rotation matrix of $\frac{\pi}{2}$ about $\boldsymbol{u}_i$.

As indicated in the above section, the manipulator is at singular configurations when $\boldsymbol{w}_i = \boldsymbol{u}_i$ for any $i = 1, 2, 3$. This will be intensively studied in the following section. Thus, in equation (10), it is supposed that $\boldsymbol{w}_i$ is not perpendicular to $\mathscr{P}_i$, namely $(\mathbf{I}_3 - \boldsymbol{u}_i\boldsymbol{u}_i^T)\boldsymbol{w}_i \neq 0$.

By substituting equation (8) into equation (10), the closed-form solutions of the unit vectors $\boldsymbol{v}_i$ can be derived as

$$\begin{cases} \boldsymbol{v}_1 = \frac{1}{\sqrt{1-w_{1,x}^2}}\left[0,\ w_{1,z},\ -w_{1,y}\right]^T \\ \boldsymbol{v}_2 = \frac{1}{\sqrt{1-w_{2,y}^2}}\left[-w_{2,z},\ 0,\ w_{2,x}\right]^T \\ \boldsymbol{v}_3 = \frac{1}{\sqrt{1-w_{3,z}^2}}\left[w_{3,y},\ -w_{3,x},\ 0\right]^T \end{cases} \tag{11}$$

Since $\boldsymbol{v}_i, i = 1,2,3$ are parallel to the crank links in the limbs, the angular inputs of the corresponding parallelogram linkages can be obtained directly as

$$\begin{cases} \varphi_1 = \arctan 2\left(-w_{1,y}, w_{1,z}\right) \\ \varphi_2 = \arctan 2\left(-w_{2,z}, w_{2,x}\right) \\ \varphi_3 = \arctan 2\left(-w_{3,x}, w_{3,y}\right) \end{cases} \tag{12}$$

where the function $\arctan 2(\cdot)$ can identify the cranks' input angle (within the lying plane $\mathscr{P}_i$) in a whole range of $(-\pi, \pi]$ according to the components of $\boldsymbol{v}_i$.

Therefore, given any nonsingular configuration (orientation) for the manipulator's moving platform, the required angular inputs of the parallelogram linkages can be uniquely determined according to the closed-form solution (12).

In order to validate the above derivations, a numerical example is given. Here, the dimensional parameters r_0 and l_0 are set to 80 mm and 238.2 mm, respectively. Eight random configurations are given and the corresponding angular inputs are calculated out. The results are listed in Table 1. It should be noted that all the results have been validated by the widely used commercial software SOLDWORKS® and the results are completely consistent in consideration of the calculation error from computer.

Inverse Jacobian matrix

By differentiating equation (12), the input velocities of the parallelogram linkages' cranks can be represented in terms of the derivatives of $\boldsymbol{w}_i$ as

$$\begin{cases} \dot{\varphi}_1 = \frac{1}{w_{1,y}S_{\varphi_1} - w_{1,z}C_{\varphi_1}}\left[0,\ C_{\varphi_1},\ S_{\varphi_1}\right]\dot{\boldsymbol{w}}_1 \\ \dot{\varphi}_2 = \frac{1}{w_{2,z}S_{\varphi_2} - w_{2,x}C_{\varphi_2}}\left[S_{\varphi_2},\ 0,\ C_{\varphi_2}\right]\dot{\boldsymbol{w}}_2 \\ \dot{\varphi}_3 = \frac{1}{w_{3,x}S_{\varphi_3} - w_{3,y}C_{\varphi_3}}\left[C_{\varphi_3},\ S_{\varphi_3},\ 0\right]\dot{\boldsymbol{w}}_3 \end{cases} \tag{13}$$

where $\dot{\boldsymbol{w}}_i = [\dot{w}_{i,x}, \dot{w}_{i,y}, \dot{w}_{i,z}]^T, i = 1,2,3$

According to equation (8), the derivatives $\dot{\boldsymbol{w}}_i, i = 1,2,3$ can be obtained readily in terms of the moving platform's rotational velocity as

$$\begin{cases} \dot{\boldsymbol{w}}_1 = \dot{\mathbf{R}}_{st}\mathbf{R}_{st}^T\mathbf{R}_{st}\boldsymbol{e}_2 = \omega \times \boldsymbol{w}_1 = -\boldsymbol{w}_1 \times \omega \\ \dot{\boldsymbol{w}}_2 = \dot{\mathbf{R}}_{st}\mathbf{R}_{st}^T\mathbf{R}_{st}\boldsymbol{e}_3 = \omega \times \boldsymbol{w}_2 = -\boldsymbol{w}_2 \times \omega \\ \dot{\boldsymbol{w}}_3 = \dot{\mathbf{R}}_{st}\mathbf{R}_{st}^T\mathbf{R}_{st}\boldsymbol{e}_1 = \omega \times \boldsymbol{w}_3 = -\boldsymbol{w}_3 \times \omega \end{cases} \tag{14}$$

where $\omega = [\omega_1, \omega_2, \omega_3]^T \in \mathbb{R}^3$ denotes the rotational velocity of the manipulator's moving platform with respect to {S}. And $\omega\times = \dot{\mathbf{R}}_{st}\mathbf{R}_{st}^T$ represents the cross-product operator of ω, which can be expressed by a 3×3 antisymmetric matrix. Likewise, $\boldsymbol{w}_i\times$ can also be written by a 3×3 anti-symmetric matrix, as

$$\hat{\mathbf{w}}_i = \boldsymbol{w}_i\times = \begin{bmatrix} 0 & -w_{i,3} & w_{i,2} \\ w_{i,3} & 0 & -w_{i,1} \\ -w_{i,2} & w_{i,1} & 0 \end{bmatrix}$$

As a result, the inverse Jacobian matrix can be obtained by substituting equation (14) into equation (13) as

$$\dot{\varphi} = \mathbf{J}^{-1}\omega \Rightarrow \mathbf{J}^{-1} = \begin{bmatrix} a_{11}, & a_{12}, & a_{13} \\ a_{21}, & a_{22}, & a_{23} \\ a_{31}, & a_{32}, & a_{33} \end{bmatrix} \tag{15}$$

Table 1. Results of inverse kinematics for eight random configurations.

Random configuration (deg)			Angular inputs (deg)		
s_1	s_2	s_3	φ_1	φ_2	φ_3
16.5554	−12.4608	18.5511	−75.0000	−99.8904	−73.1431
11.8501	−16.1856	13.5813	−80.0000	−104.8992	−77.8273
17.0676	−17.0676	−18.1412	−70.0000	−109.8865	−110.8401
−26.9084	−15.5084	19.6698	−120.0000	−111.0575	−67.1954
−29.6726	−29.6726	−18.9035	−115.0000	−117.1803	−101.5948
3.9268	9.4801	−44.8833	−90.0000	−82.8929	−135.0000
−9.2803	15.5084	−32.0131	−105.0000	−72.7163	−123.6816
−41.2252	24.4448	−20.9387	−135.0000	−53.8398	−118.3348

where $\dot{\varphi} = [\dot{\varphi}_1, \dot{\varphi}_2, \dot{\varphi}_3]^T$ represents the vector of the cranks' input velocities. And the components of the inverse Jacobian matrix $\mathbf{J}^{-1}$ can be given by

$$\begin{cases} a_{11} = 1, \ a_{12} = \frac{-w_{1,x}S_{\varphi_1}}{w_{1,y}S_{\varphi_1} - w_{1,z}C_{\varphi_1}}, \ a_{13} = \frac{w_{1,x}C_{\varphi_1}}{w_{1,y}S_{\varphi_1} - w_{1,z}C_{\varphi_1}} \\ a_{21} = \frac{w_{2,y}C_{\varphi_2}}{w_{2,z}S_{\varphi_2} - w_{2,x}C_{\varphi_2}}, \ a_{22} = 1, \ a_{23} = \frac{-w_{2,y}S_{\varphi_2}}{w_{2,z}S_{\varphi_2} - w_{2,x}C_{\varphi_2}} \\ a_{31} = \frac{-w_{3,z}S_{\varphi_3}}{w_{3,x}S_{\varphi_3} - w_{3,y}C_{\varphi_3}}, \ a_{32} = \frac{w_{3,z}C_{\varphi_3}}{w_{3,x}S_{\varphi_3} - w_{3,y}C_{\varphi_3}}, \ a_{33} = 1 \end{cases}$$

Singularity analysis

In this section, the singularity of the proposed SPM is analyzed. Firstly, the singularity of the parallelogram of each limb is analyzed. Secondly, the singularity mentioned in the above section is analyzed, where the axis of revolute joint moves to a parallel position to the first axis of the corresponding universal one. As is shown in Figure 4, when the input angle $\phi_i = 0^\circ$ or 180°, the parallelogram linkage C_iD_i is coincident with A_iB_i. Then if angle ϕ_i is driven to rotate, the point C_i may move in two directions. Thus, the parallelogram is singular at these two positions. To avoid this kind of singularity, the input angles ϕ_i are restraint to be more than 0° and less than 180°.

The approach of analyzing singularity in Li and McCarthy[29] and Kong and Gosselin[30] is a systematic approach. However, for the proposed SPM in this paper, it is difficult to get analytical solution for the input angles ϕ_i. By contrast, the singularity of the proposed SPM can be easily identified by observation and the singular poses can be described conveniently. Thus in this paper, the observation method is utilized. The results are the same with that in Li and McCarthy[29] and Kong and Gosselin.[30] The second kind of singularity occurs when $\boldsymbol{w}_i = \pm \boldsymbol{e}_i$. Let $\boldsymbol{w}_1 = \pm \boldsymbol{u}_1$, such that $w_{2,x} = w_{3,x} = 0$. Then, it yields $\boldsymbol{v}_2 = \boldsymbol{v}_3 = \boldsymbol{u}_1$ according to equation (11). Meanwhile, the direction of $\boldsymbol{v}_1$ can be arbitrarily selected as $\boldsymbol{w}_1$ is perpendicular to $\mathscr{P}_1$. It indicates that, in such a situation, the moving platform can freely rotate itself about $\boldsymbol{w}_1$ axis, without changing the configuration of Pa-linkages, as shown in Figure 5. In other words, the moving platform's rotational motion about the $\boldsymbol{w}_1$ axis is not controllable any more.

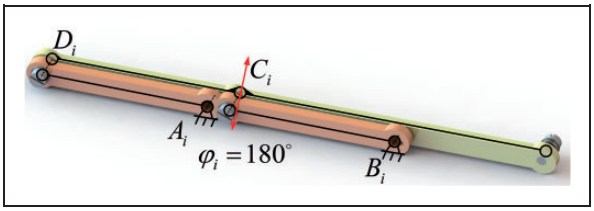

Figure 4. The singular position of the parallelogram of each limb.

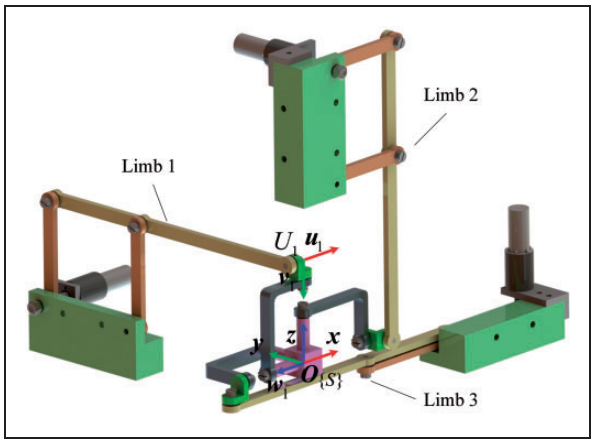

Figure 5. One singularity configuration of the 3-PaUR parallel manipulator when $\boldsymbol{w}_1 = \pm \boldsymbol{u}_1$.

By solving equation (9), the corresponding configurations can be presented by the canonical coordinates $\boldsymbol{s}$, in the form of parametric functions as

$$\begin{cases} \boldsymbol{w}_1 = \quad \boldsymbol{u}_1 \Rightarrow \begin{cases} s'_3 = -\sqrt{\frac{1+C_\theta}{1-C_\theta}} \\ s'_1 = s'_2 = \pm\sqrt{\frac{-C_\theta}{1-C_\theta}} \end{cases} \\ \boldsymbol{w}_1 = -\boldsymbol{u}_1 \Rightarrow \begin{cases} s'_3 = \sqrt{\frac{1+C_\theta}{1-C_\theta}} \\ s'_1 = -s'_2 = \pm\sqrt{\frac{-C_\theta}{1-C_\theta}} \end{cases} \end{cases} \tag{16}$$

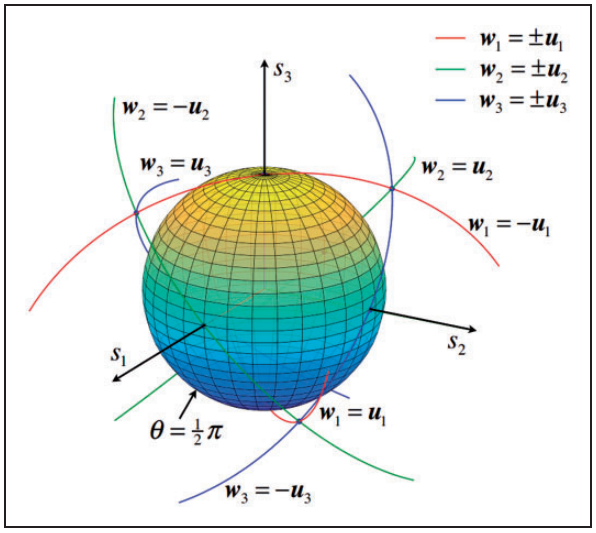

Figure 6. Singularity configurations of the 3-PaUR parallel manipulator within its rotational workspace.

where $\theta \in [\frac{1}{2}\pi, \pi)$.

From equation (16), two spatial curves can be derived as shown in Figure 6. The configurations associated with the points on them are suffering from a singularity as illustrated in Figure 5. In such a case, the actuation φ_1 only introduces a self-motion to the first limb, but does not change the configuration of the moving platform.

Analogously, for the situation $\boldsymbol{w}_2 = \pm\, \boldsymbol{u}_2$ and $\boldsymbol{w}_3 = \pm\, \boldsymbol{u}_3$, the parallel manipulator loses the control of the moving platform's rotational capability about the $\boldsymbol{w}_2$ and $\boldsymbol{w}_3$ axis, respectively. Similar to equation (16), the corresponding configurations can be derived as

$$\begin{cases} \boldsymbol{w}_2 = \quad \boldsymbol{u}_2 \Rightarrow \begin{cases} s'_1 = -\sqrt{\frac{1+C_\theta}{1-C_\theta}} \\ s'_2 = s'_3 = \pm\sqrt{\frac{-C_\theta}{1-C_\theta}} \end{cases} \\ \boldsymbol{w}_2 = -\boldsymbol{u}_2 \Rightarrow \begin{cases} s'_1 = \quad \sqrt{\frac{1+C_\theta}{1-C_\theta}} \\ s'_2 = -s'_3 = \pm\sqrt{\frac{-C_\theta}{1-C_\theta}} \end{cases} \\ \boldsymbol{w}_3 = \quad \boldsymbol{u}_3 \Rightarrow \begin{cases} s'_2 = -\sqrt{\frac{1+C_\theta}{1-C_\theta}} \\ s'_3 = s'_1 = \pm\sqrt{\frac{-C_\theta}{1-C_\theta}} \end{cases} \\ \boldsymbol{w}_3 = -\boldsymbol{u}_3 \Rightarrow \begin{cases} s'_2 = \quad \sqrt{\frac{1+C_\theta}{1-C_\theta}} \\ s'_3 = -s'_1 = \pm\sqrt{\frac{-C_\theta}{1-C_\theta}} \end{cases} \end{cases} \tag{17}$$

As a result, totally three pairs of curves can be achieved, as shown in Figure 6, to represent all potential singular configurations of the proposed spherical parallel manipulator. As indicated in the above, each pair of them relates to the a particular type of singularity corresponding to $\boldsymbol{w}_i = \pm\, \boldsymbol{u}_i$.

At the intersections of these curves, the rotational mobility of the moving platform is totally out of control. It means, in such a configuration, the manipulator's moving platform will keep still when the limbs' inputs change as shown in Figure 7. And the canonical coordinates corresponding to these singular configurations can be represented as

$$\begin{cases} \boldsymbol{s}_{*,1} = \frac{2\sqrt{3}\pi}{9}\,[1, \quad 1, -1]^T \\ \boldsymbol{s}_{*,2} = \frac{2\sqrt{3}\pi}{9}\,[-1, -1, -1]^T \\ \boldsymbol{s}_{*,3} = \frac{2\sqrt{3}\pi}{9}\,[-1, \quad 1, \quad 1]^T \\ \boldsymbol{s}_{*,4} = \frac{2\sqrt{3}\pi}{9}\,[1, -1, \quad 1]^T \end{cases} \tag{18}$$

where $\theta = \frac{2}{3}\pi$.

Meanwhile, the singularity property can also be verified by the mobility analysis of the studied parallel manipulator. In the case of $\boldsymbol{w}_i = \pm\, \boldsymbol{u}_i$, the twist system of the corresponding limb will degenerate to a third-order screw system due to the condition $\boldsymbol{S}_{i,4} = \boldsymbol{S}_{i,1}$. Accordingly, the limb's constraint screw system can be obtained as

$$\mathbb{S}_i^r = \mathrm{span}\left\{\boldsymbol{S}_{i,1}^r, \boldsymbol{S}_{i,2}^r, \boldsymbol{S}_{i,3}^r\right\} \tag{19}$$

where $\boldsymbol{S}_{i,1}^r$ and $\boldsymbol{S}_{i,2}^r$ are as same as those defined in (2). While $\boldsymbol{S}_{i,3}^r = \begin{bmatrix} \boldsymbol{v}_i \times \boldsymbol{u}_i \\ \boldsymbol{0} \end{bmatrix}$ corresponds to a pure torque constraint perpendicular to the $\boldsymbol{u}_i\boldsymbol{v}_i$ plane.

Comparing with the original constraint system (5), $\boldsymbol{S}_{i,3}^r$ becomes an extra base element of $\mathbb{S}^r$

$$\mathbb{S}^r = \left\{\boldsymbol{S}_1^r, \boldsymbol{S}_1^r, \boldsymbol{S}_3^r, \boldsymbol{S}_4^r\right\} \tag{20}$$

where $\boldsymbol{S}_4^r = \boldsymbol{S}_{i,3}^r$.

As a result, the final twist system of the moving platform yields

$$\mathbb{S} = \left\{\boldsymbol{S}_1', \boldsymbol{S}_2'\right\} \tag{21}$$

which corresponds to a 2-DOF rotational system.

Further, when the proposed parallel manipulator is at a configuration associated with $\boldsymbol{s}_{*,j}$ for any $j = 1,2,3,4$, all the three limbs will be constrained by third-order screw system. And the union of these systems spans the whole screw space. In other words, the moving platform will be fully constrained and is not controlled by the actuators.

As analyzed in this section, all singular configurations of the proposed 3-PaUR parallel manipulator can be illustrated in its rotational workspace in an intuitive manner, as shown in Figure 6. Then, for a particular task, path planning can be performed for the manipulator to avoid these undesirable configurations.

Manipulability analysis

In this section, the determinate of Jacobian matrix is used as the manipulability index[31] to evaluate the

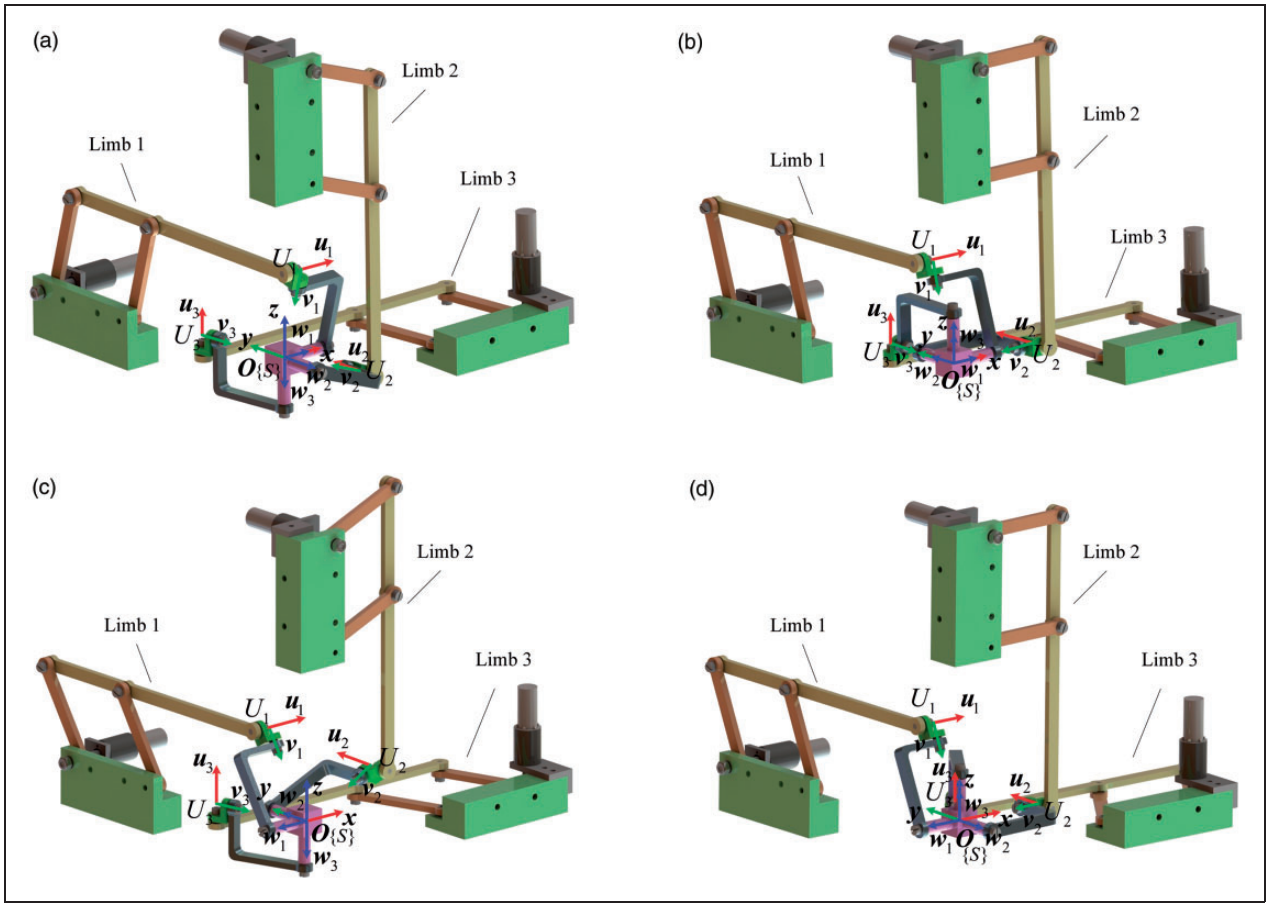

Figure 7. All the four kinds of singularity configurations of the 3-PaUR parallel manipulator within its rotational workspace: (a) $S_{*,1}$: $\boldsymbol{w}_1 = \boldsymbol{u}_1$, $\boldsymbol{w}_2 = -\boldsymbol{u}_2$, $\boldsymbol{w}_3 = -\boldsymbol{u}_3$; (b) $S_{*,2}$: $\boldsymbol{w}_1 = \boldsymbol{u}_1$, $\boldsymbol{w}_2 = \boldsymbol{u}_2$, $\boldsymbol{w}_3 = \boldsymbol{u}_3$; (c) $S_{*,3}$: $\boldsymbol{w}_1 = -\boldsymbol{u}_1$, $\boldsymbol{w}_2 = \boldsymbol{u}_2$, $\boldsymbol{w}_3 = -\boldsymbol{u}_3$; (d) $S_{*,4}$: $\boldsymbol{w}_1 = -\boldsymbol{u}_1$, $\boldsymbol{w}_2 = -\boldsymbol{u}_2$, $\boldsymbol{w}_3 = \boldsymbol{u}_3$.

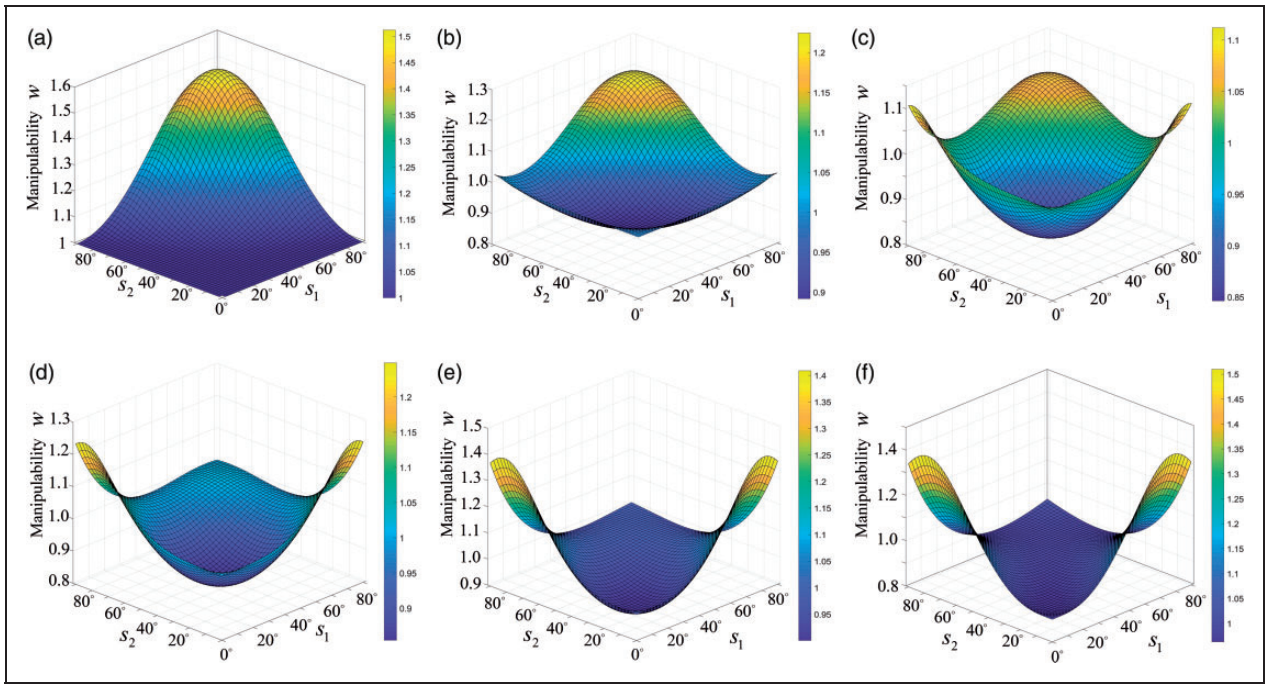

Figure 8. The results of the six 2D workspaces' manipulability analysis: (a) $s_3 = 0^\circ$; (b) $s_3 = 15^\circ$; (c) $s_3 = 30^\circ$; (d) $s_3 = 45^\circ$; (e) $s_3 = 60^\circ$; and (f) $s_3 = 75^\circ$.

dexterity performance of the studied manipulator, namely

$$w = |det(\mathbf{J}^{-1})| \tag{22}$$

Here, six 2D workspaces are selected to analyze the manipulability, which are

$$\begin{cases} 0 \leqslant s_1 \leqslant 90^\circ \\ 0 \leqslant s_2 \leqslant 90^\circ \\ s_3 = 0^\circ, 15^\circ, 30^\circ, 45^\circ, 60^\circ, 75^\circ \end{cases} \tag{23}$$

It should be noted that, within the workspaces, there are no singular configurations.

The corresponding results are illustrated in Figure 8(a) to (f), respectively. The results show that when s_3 is about less than 30°, the manipulability is higher at the configuration of $s_1 = s_2 = 80^\circ$. When s_3 is more than 30°, the manipulability reaches highest at the configurations of $s_1 = 0^\circ, s_2 = 80^\circ$ and $s_1 = 80^\circ, s_2 = 0^\circ$. Meanwhile, the surfaces of the results are smooth, and the minimum manipulability is about 0.8 and the maximum about 1.55. The difference between the minimum and maximum is not big, which indicates a relatively good performance of force transmission.

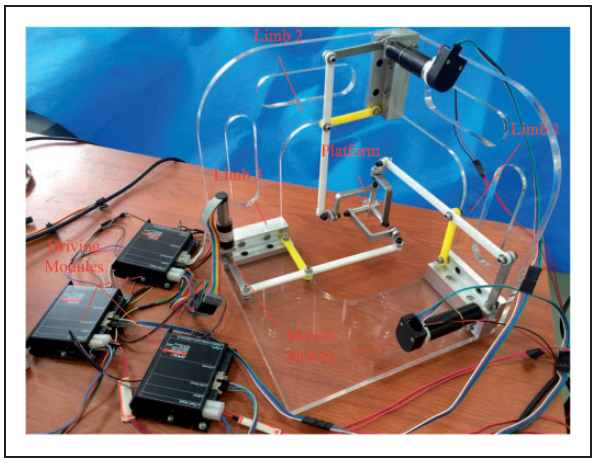

Figure 9. The fabricated prototype.

Prototype and validation

In this section, to demonstrate the feasibility and effectiveness of the design, one prototype is fabricated as shown in Figure 9. The dimensional parameters r_0 and l_0 are set as 80 mm and 238.2 mm, respectively, which are the same as that in the "Inverse kinematics" section. The three limbs are perpendicular to each other. The drive motors (Maxon motors) are mounted on the crank links of the Pa-linkages.

To display the good rotation ability, an experiment is conducted. One laser device is mounted on the platform. The emission direction of the laser is $\boldsymbol{V}_l = (-1, -1, -1)$, which is also set as the rotation axis. As shown in Figure 10, the initial input angles $\varphi_i (i = 1, 2, 3)$ are all set to 0. The crank links of the three limbs rotate 6° simultaneously from the present frame to the next one. From the results we can see that the red laser point on the white paper is still when the platform rotates about the $\boldsymbol{V}_l$ axis, which validate the good rotation ability of the SPM.

However, there are also limitations for the proposed SPM. The L-type link is used to connect the universal joint and revolute joint, so that the load capacity of the platform is not high. As indicated in Wu et al.,[32] the stiffness of the limbs of the SPM has influences on the orientation accuracy and the center of the platform may shift away from the initial position. Meanwhile, the dimensional parameters are not optimized and there are interferences between the links for some specified poses.

In the future, we will optimize the structure of the proposed SPM to avoid interferences and enlarge the workspace. Meanwhile, we will derive the stiffness model to analyze the orientation accuracy and center shift of the proposed SPM. The dimensional

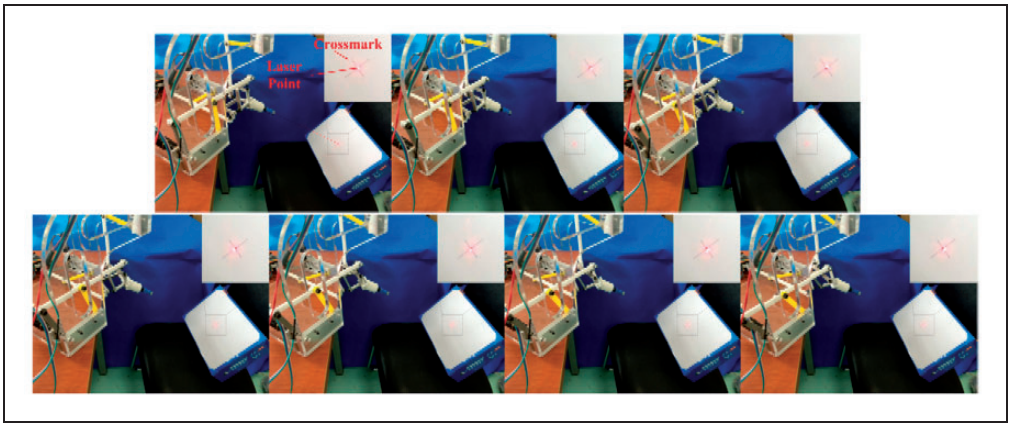

Figure 10. The results of the experiment, all the links rotate 6° simultaneously from the present frame to the next one.

parameters can be further optimized. After corresponding modifications, possible applications to celestial orientation and rehabilitation devices will be considered.

Conclusions

This paper presents a new type of 3-DOF SPM which is comprised of planar parallelogram linkage. We analyze in detail the kinematics of the proposed SPM. Its mobility is validated by taking advantage of the reciprocal screws. The inverse kinematics is investigated and the closed-form solution is derived, based on which, the inverse Jacobian matrix is derived. The singularity configurations of the SPM within its rotational workspace are all investigated. After that, the manipulability is analyzed and the results show that the SPM has a relatively good performance of force transmission. In the end, one prototype is fabricated and one simple experiment is conducted to validate the feasibility of the design and the correctness of the derivations.

Declaration of Conflicting Interests

The author(s) declared no potential conflicts of interest with respect to the research, authorship, and/or publication of this article.

Funding

The author(s) disclosed receipt of the following financial support for the research, authorship, and/or publication of this article: This work was supported by the National Science Foundation of China (NSFC) [Grant nos. 51505279, 11472172, and 51421092], and the National Basic Research Program of China (973 Program) [research grant 2014CB046600].

ORCID iD

Weidong Yu http://orcid.org/0000-0003-4918-5977

References

1. Gosselin C and Angeles J. The optimum kinematic design of a spherical three-degree-of-freedom parallel manipulator. *J Mech Transm Autom Des* 1989; 111: 202–207.
2. Gosselin CM and Hamel JF. The agile eye: A high-performance three-degree-of-freedom camera-orienting device. In: *Proceedings of 1994 IEEE international conference on robotics and automation*, 1994, pp.781–786. New York: IEEE.
3. Vischer P and Clavel R. Argos: A novel 3-dof parallel wrist mechanism. *Int J Robot Res* 2000; 19: 5–11.
4. Di Gregorio R. Kinematics of a new spherical parallel manipulator with three equal legs: The 3-URC wrist. *J Robot Syst* 2001; 18: 213–219.
5. Di Gregorio R. A new parallel wrist using only revolute pairs: the 3-RUU wrist. *Robotica* 2001; 19: 305–309.
6. Di Gregorio R. The 3-RRS wrist: A new, simple and non-overconstrained spherical parallel manipulator. *Trans-Am Soc Mech Engrs J Mech Des* 2004; 126: 850–855.
7. Di Gregorio R. A new family of spherical parallel manipulators. *Robotica* 2002; 20: 353–358.
8. Karouia M and Hervé J. A three-DOF tripod for generating spherical rotation. In: *Advances in robot kinematics*. New York: Springer, 2000, pp.395–402.
9. Karouia M and Hervé JM. A family of novel orientational 3-dof parallel robots. In: *Romansy 14*. New York: Springer, 2002, pp.359–368.
10. Li Q and Huang Z. A family of symmetrical lower-mobility parallel mechanisms with spherical and parallel subchains. *J Field Robot* 2003; 20: 297–305.
11. Kong X and Gosselin CM. Type synthesis of three-degree-of-freedom spherical parallel manipulators. *Int J Robot Res* 2004; 23: 237–245.
12. Fang Y and Tsai LW. Structure synthesis of a class of 3-dof rotational parallel manipulators. *IEEE Trans Robot Autom* 2004; 20: 117–121.
13. Karouia M and Hervé JM. Asymmetrical 3-dof spherical parallel mechanisms. *Eur J Mech-A/Solids* 2005; 24: 47–57.
14. Karouia M and Hervé JM. Non-overconstrained 3-dof spherical parallel manipulators of type: 3-RCC, 3-CCR, 3-CRC. *Robotica* 2006; 24: 85–94.
15. Gallardo J, Rodríguez R, Caudillo M, et al. A family of spherical parallel manipulators with two legs. *Mech Mach Theory* 2008; 43: 201–216.
16. Daniali HM, Zsombor-Murray P and Angeles J. The kinematics of 3-dof planar and spherical double-triangular parallel manipulators. In: *Computational kinematics*. New York: Springer, 1993, pp.153–164.
17. Enferadi J and Tootoonchi AA. A novel spherical parallel manipulator: forward position problem, singularity analysis, and isotropy design. *Robotica* 2009; 27: 663–676.
18. Huda S, Takeda Y and Hanagasaki S. Kinematic design of 3-URU pure rotational parallel mechanism to perform precise motion within a large workspace. *Meccanica* 2011; 46: 89–100.
19. Callegari M, Carbonari L, Palmieri G, et al. Parallel wrists for enhancing grasping performance. In: *Grasping in robotics*. New York: Springer, 2013, pp.189–219.
20. Lin R, Guo W and Gao F. Type synthesis of a family of 3-dof spherical parallel mechanisms using upper-lower combination and axis movement theorem. In: *Advances in reconfigurable mechanisms and robots II*. New York: Springer, 2016, pp.315–326.
21. Enferadi J and Shahi A. On the position analysis of a new spherical parallel robot with orientation applications. *Robot Comput-Integr Manuf* 2016; 37: 151–161.
22. Yang G, Ho H, Lin W, et al. A differential geometry approach for the workspace analysis of spherical parallel manipulators. In: Tian Huang (ed.) *11th world congress in mechanism and machine science*, Tianjin, China, 18–21 August 2003, pp.1–4. China: China Machinery Press.
23. Vertechy R and Parenti-Castelli V. Real-time direct position analysis of parallel spherical wrists by using extra sensors. *J Mech Des* 2006; 128: 288–294.
24. Merlet JP. *Parallel robots*. Vol. 74, New York: Springer Science & Business Media, 2012.

25. Hunt KH. *Kinematic geometry of mechanisms*. London: Oxford University Press, 1978.
26. Dai JS, Huang Z and Lipkin H. Mobility of overconstrained parallel mechanisms. *J Mech Des* 2006; 128: 220–229.
27. Joshi SA and Tsai LW. Jacobian analysis of limited-DOF parallel manipulators. *J Mech Des* 2002; 124: 254–258.
28. Murray RM, Sastry SS and Li ZX. *A mathematical introduction to robotic manipulation*. Boca Raton, FL: CRC Press, Inc., 1994.
29. Li J and McCarthy JM. Analysis of two spherical parallel manipulators with hidden revolute joints. *J Mech Robot* 2017; 9: 031007.
30. Kong X and Gosselin CM. A formula that produces a unique solution to the forward displacement analysis of a quadratic spherical parallel manipulator: The agile eye. *J Mech Robot* 2010; 2: 044501.
31. Yoshikawa T. Manipulability of robotic mechanisms. *Int J Robot Res* 1985; 4: 3–9.
32. Wu G, Bai S and Kepler J. Mobile platform center shift in spherical parallel manipulators with flexible limbs. *Mech Mach Theory* 2014; 75: 12–26.